Particle & Particle Systems Characterization
www.particle-journal.com

Development of a Liver-Targeting Gold–PEG–Galactose Nanoparticle Platform and a Structure–Function Study

Ya Ding, Juan-Juan Liang, Dong-Dong Geng, Di Wu, Lei Dong, Wen-Bin Shen, Xing-Hua Xia, and Can Zhang**

For the specific liver parenchymal cell delivery, a series of short heterobifunctional poly(ethylene glycol) (PEG) derivatives containing dimercapto and galactose (Gal) terminals is synthesized for the preparation of gold conjugates. The Gal density on the surface of all gold conjugates can be well controlled and the prepared gold conjugates are stable in various media, even in the presence of serum. For the liver targeting and reflectance imaging applications, the structure–function relationships of this platform, including the influence of the PEG molecular weight and the Gal ligand coverage of hybrid particles on the cytotoxicity and cellular recognition of tumor cells in vitro and on their liver-targeting ability in small animals, are studied. Biocompatibility results show that HepG2 cells are more sensitive than HeLa cells to gold conjugates. Cellular uptake studies demonstrate that a lower PEG molecular weight, a higher Gal density, or a higher gold concentration can increase the cellular uptake efficiency of these hybrid particles in HepG2 cells when the other parameters are constant. The results reveal the importance of parameter modulation for the design and control of nanoprobes and the gold conjugates with short PEG chains and a high Gal density are a potential vector for active-targeting therapy.

1. Introduction

Conjugation of drugs to gold nanoparticles (AuNPs) is a promising approach to improve the effectiveness of drugs by controlling their natural properties.[1–3] For in vivo preferential hepatocyte delivery, sugar-functionalized spherical gold nanoparticles with a 3D polyvalent carbohydrate structure have been designed and used as a novel system for optimal targeting formulations.[4,5] This strategy provides an alternative method to compensate for the extremely low affinity of the biological interactions where carbohydrates are involved through multivalent presentation of the ligands.[6–8]

For the preparation of sugar-functionalized gold nanoparticles, two methods are commonly used: 1) the reduction of gold salts in the presence of polymer derivatives that contain covalently attached carbohydrate structures[9,10] and 2) post-treatment of the gold nanoparticles by surface modification via thiol-functionalized ligands that bear a sugar moiety.[11–13] To improve the active liver-targeting ability and simultaneously reduce the cytotoxicity of sugar-functionalized gold nanoparticles in vivo and in vitro, several parameters including particle size, surface property, and specific targeting must be taken into account. However, there are several contradictions in the process of regulating the various parameters, and the optimized liver-targeting nanoprobe and nanoparticle-based delivery vehicle are still challenging.

From the anatomical structure of liver, liver parenchymal cells (PC) are situated behind a fenestrated endothelium. Thus, only particles small enough can pass through the hepatic sinusoidal structural barriers, and subsequently arrive in the liver cells.[12] In order to restrict the size of the gold conjugates, both the particle size of the gold core and the thickness of the modified organic layer must be considered. For the particle size, however, it has been reported that gold nanoparticles with small sizes (less than 10 nm) showed the most widespread organ distribution, including distribution in the blood, liver, spleen, kidney, testis, thymus, heart, lung, and brain.[13] Therefore, modifying the surface of gold nanoparticles with both biocompatible polymeric molecules and specific site-targeting moieties will grant the nanogold a long circulation character and active target function.

Thus, the utilization of a hydrophilic polymer stabilizer, such as poly(ethylene glycol) (PEG), becomes extensively as an effective way to prevent particle aggregation and prolong the circulation time of nanoparticles in vivo, especially those modified by PEG with a molecular weight (MW) greater than 2000 Da.[14,15] It has been reported that the long chains of hydrophilic PEG polymer sterically stabilized the nanoparticles against opsonization. However, the long chain of PEG molecules with high MW will increase the thickness of outer organic layer of gold nanoparticles, and subsequently increase the particle size of gold

Dr. Y. Ding, J.-J. Liang, D.-D. Geng, D. Wu,
Prof. W.-B. Shen, Prof. C. Zhang
State Key Laboratory of Natural Medicines
Department of Pharmaceutical Analysis
China Pharmaceutical University
Nanjing, 210009, China
E-mail: zhangcan@cpu.edu.cn
Prof. L. Dong, Prof. X.-H. Xia
State Key Laboratory of Analytical Chemistry for Life Science
School of Chemistry and Chemical Engineering
Nanjing University, Jiangsu, 210093, China
E-mail: xhxia@nju.edu.cn

DOI: 10.1002/ppsc.201300120

© 2013 WILEY-VCH Verlag GmbH & Co. KGaA, Weinheim

conjugates. And the hydrophilicity and mobility characteristics of particle surfaces reduce the recognition capability of modified nanoparticles by circulating macrophages of the liver.[16,17] For this reason, reducing the molar weight of PEG on the gold surface is expected to be most likely an appropriate approach to reduce the particle size of gold conjugates, and then enhance the liver recognition capability for gold nanoparticles.[18] However, the possible long circulation character of the gold nanoparticles modified by relatively short PEG molecules (no more than 1000 Da) in vivo has rarely been studied.

In addition, the hepatocyte delivery mechanism has been found to be closely related to the high affinity and rapid internalization rate of asialoglycoprotein receptor (ASGPR)-mediated endocytosis.[19,20] It has been reported that several sugar ligands (galactose, *N*-acetylgalactosamine, mannose, lactose, and sialic acid)[21] interact with ASGPR to various extents. Among them, galactose-grafted materials show a greater affinity for ASGPR in liver tumor cells.[22] The studies have demonstrated that the binding affinity of a carbohydrate ligand to the ASGPR highly correlates with the degree of galactose modification. Thus, precise regulation of the relative density of galactose moiety on the surface of gold nanoparticles may control the affinity and recognition ability of the resultant gold conjugates in liver parenchymal cells.

In the present work, to obtain optimal galactose-functionalized gold nanoparticles for liver targeting as a drug delivery vector, we propose a simple strategy for the synthesis of a series of short heterobifunctional PEG derivatives (MWs = 400, 600, and 1000 Da) containing dimercapto and galactose (Gal) terminals. Gold conjugates with a gold core of ca. 5 nm with different low PEG MWs and galactose densities have been prepared. Different from the previous reports,[11,23] the present work will focus on how much the low MWs of PEG and the galactose density on gold nanoparticles influence the cytotoxicity, cell recognition, and biodistribution of these types of liver-targeting gold conjugates. The results reveal the importance of parameter modulation in the design and control of nanoconjugate-based drug delivery system and indicate that the Au conjugates with short PEG chains and a high Gal density is a promising vector for active-targeting therapy, especially for the treatment of liver disease and liver cancer therapy.

2. Results and Discussion

2.1. The Synthesis and Characterization of Au–PEG–Gal Conjugates

The synthesis processes of ligands and Au–PEG–Gal conjugates are illustrated in **Figure 1**. First, the ligand features an ester bond coupling thioctic acid (TA) to one terminal of PEG to form TA–PEG (PEG MW of 400, 600, and 1000 Da), which was synthesized and separated as 1) the intermediates for the synthesis of Gal-bearing PEG ligands (TA–PEG–Gal), 2) the ligand for adjusting the Gal density on the gold surface, and 3) the protective molecule for the preparation of the Au–PEG conjugate as the control of Au–PEG–Gal nanoparticles. And then, the conjugation of the Gal moiety on the other hydroxyl end-group of PEG was performed via an amino-acid-based linkage (glycine used here).[27] It provides heterobifunctional groups that allow conjugation with both the hydroxyl end of PEG and the carboxyl group of lactobionic acid (LA) via carboxyl and amino groups, respectively. Moreover, the disulfide bond in the structure of TA-containing ligands was reduced through the use of the sodium borohydride reduction method.[26] With the addition of gold nanoparticles into the reaction solution, PEG-conjugated gold nanoparticles with and without the Gal moiety are obtained via the Au–S covalent bond.[24,25] The chemical structure of gold conjugates was characterized by Fourier transform infrared (FTIR) spectroscopy.

FTIR spectra of the Au–PEG and Au–PEG–Gal conjugates are shown in **Figure 2**. For Au–PEG, absorption bands at 2933, 2873, and 1456 cm^{-1} are attributed to C–H stretching and bending vibrations of the methylene groups of dihydrolipoic acid (DHLA), respectively. The broad band in the range of 3600–3300 cm^{-1} arises from the O–H stretching vibration of the hydroxyl ends on PEG, and the absorption peak at 1104 cm^{-1} is due to the C–O stretching vibration in the PEG backbone. The absorption band at 1738 cm^{-1} is assigned to the $\upsilon_{C=O}$ vibration in the ester bond between TA and PEG. A comparison between these spectra and the FTIR spectrum of Au–PEG reveals that the gold conjugates with Gal moiety exhibit a new absorption peak of the amide I group ($\upsilon_{C=O}$) at 1659 cm^{-1} and a stronger υ_{O-H} peak between 3600 and 3300 cm^{-1}. These peaks indicate the successful substitution of the carbohydrate structure via an amide bond between the glycine and the LA.

To evaluate the percentage of Gal coverage on the gold surface, thermogravimetric analysis (TGA) and ^{1}H NMR spectra for all of the investigated gold conjugates were measured. The TGA has been carried out to evaluate the organic loss from the Au–PEG–Gal conjugate sample. The typical TGA curves of Au–PEG_{1000} (Lac0) and Au–PEG_{1000}–Gal (Lac100) were showed in **Figure 3**A, which demonstrated that the composition of the Au–PEG_{1000} conjugate was determined to be 83.02% organic and 16.98% metallic Au and Au–PEG_{1000}–Gal sample was determined to be 98.47% organic and 1.53% metallic Au. This result demonstrates that the gold surface can be covered completely by the organic layer and the increase of the organic percentage in the Au–PEG–Gal conjugate sample indicated the successful conjugation of Gal moiety on the Au surface .

In order to determine the Gal molar percentage on the gold surface, ^{1}H NMR spectra have been detected. The ^{1}H NMR spectra of Au–PEG_{1000}–Gal with TA–PEG_{1000}–Gal molar percentages of 100%, 50%, and 0% are shown in Figure 3B as representative examples. A comparison of the ^{1}H NMR spectrum of LA (not shown here) with that for Au–PEG (Lac0) results in the attribution of chemical shifts for Au–PEG_{1000}–Gal as follows: ^{1}H NMR (D_2O) δ = 4.60–3.50 (Lac, H), δ = 4.25, 3.73–3.66 (PEG, H_c), δ = 3.15 (H_a), δ = 2.48 and 1.95 (H_b), δ = 2.37 (H_g), δ = 2.27 (OH, broad), δ = 1.69 (H_d, H_f), and δ = 1.50 (H_e) ppm. Excluding the water signal at δ = 4.7 ppm, the integral ratio of the chemical shift in the lowest-field, δ = 4.53 ppm (H_1), and the proton peak at δ = 2.37 ppm, which is assigned to H_g, is used to calculate the percentage of PEG–Gal ligand on the gold surface as Equation (1).

$$\text{Gal coverage}\,(\%) = \frac{H_{1,\,\text{integral}}}{H_{g,\,\text{intergral}}/2} \times 100\% \quad (1)$$

© 2013 WILEY-VCH Verlag GmbH & Co. KGaA, Weinheim

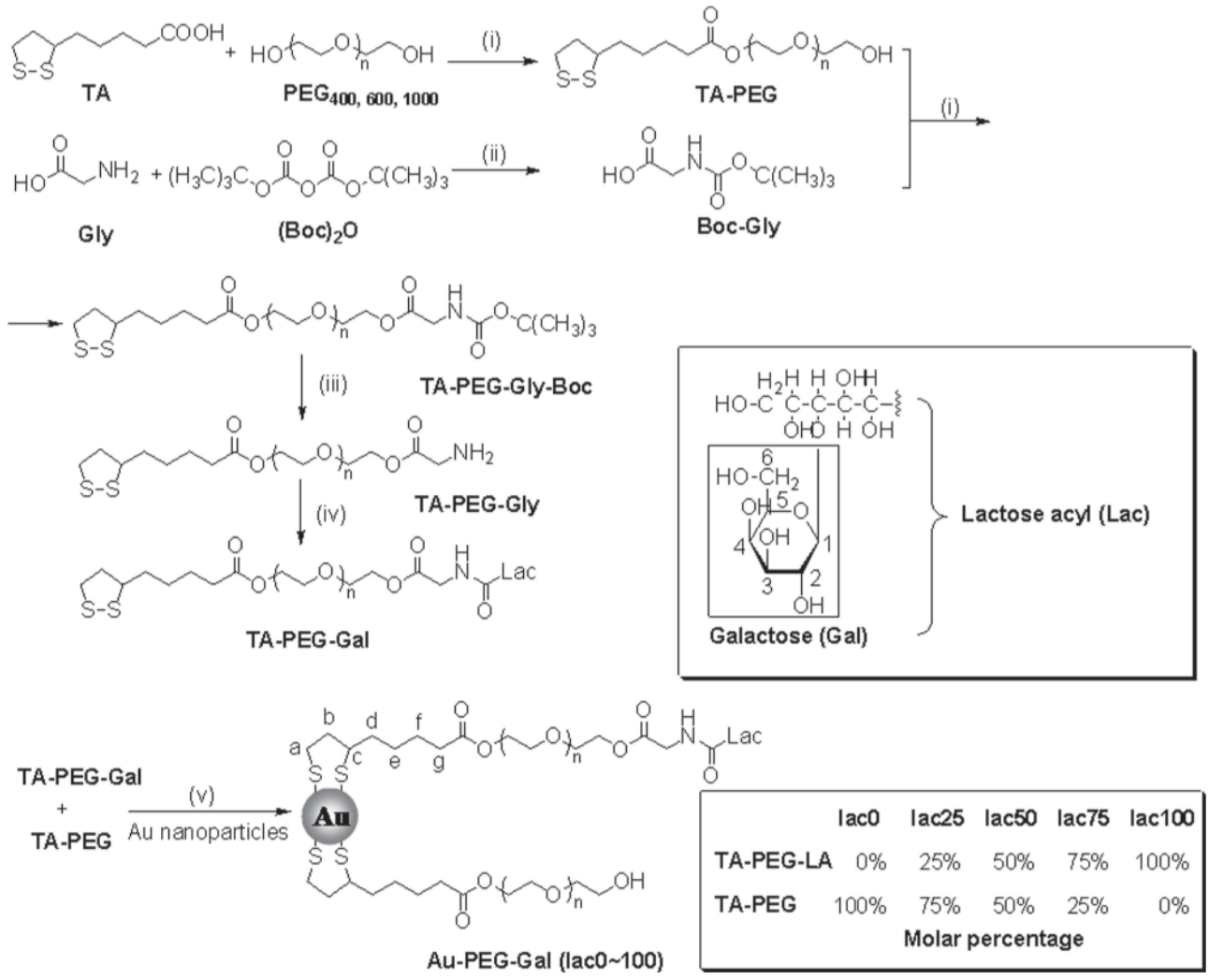

	lac0	lac25	lac50	lac75	lac100
TA-PEG-LA	0%	25%	50%	75%	100%
TA-PEG	100%	75%	50%	25%	0%

Molar percentage

Figure 1. Illustration of the syntheses of TA–PEG and TA–PEG–Gal ligands and the preparation of Au–PEG–Gal conjugates. Reagents and conditions: i) DCC, DMAP, DCM, 24 h; ii) NaOH, H_2O, THF, 15 h; iii) TFA, DCM, 3 h; iv) EDC, NHS, DMSO, 3 d; v) $NaBH_4$, MeOH, H_2O, 1 h, gold nanoparticles.

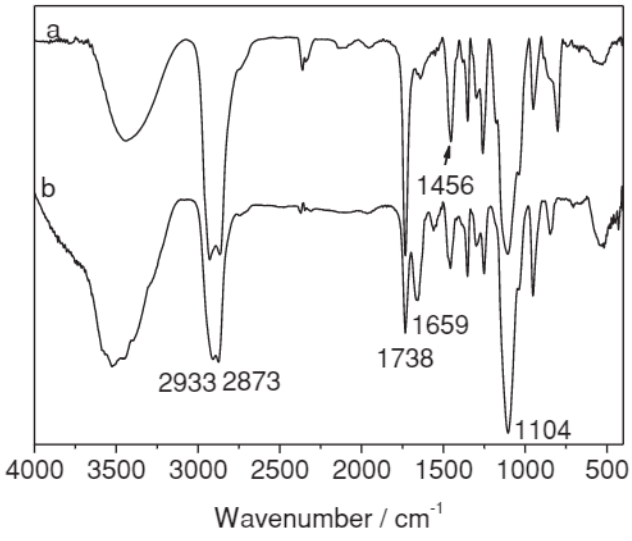

Figure 2. FTIR spectra of Au–PEG_{1000} (a) and Au–PEG_{1000}–Gal (b).

According to Equation (1), the relationship between the molar percentage of TA–PEG–Gal ($mol_{(TA–PEG–Gal)}/mol_{(TA–PEG–Gal) + (TA–PEG)}$) in the feed solution and the final Gal coverage was estimated, and results are shown in **Table 1**. In our previous work, the conjugation of galactose on one end of PEG via a direct esterification reaction between TA–PEG and LA was performed using the *N,N′*-dicyclohexylcarbodiimide (DCC)/4-dimethylaminopryidine (DMAP) catalyst. However, the reaction under these conditions is relatively slow, and no obvious product is generated even after 3 d. When a Gly spacer is inserted between the PEG and LA, the reaction speed is obviously accelerated. The substitution yield for the Gal conjugation is calculated to be ca. 60% based on the integral of the ^1H NMR spectrum when the feeding amount of TA–PEG–Gal in the solution is set to 100%. The increase in the molar percentage of TA–PEG–Gal ligand leads to an enhancement of the Gal coverage on the gold nanoparticles (shown in Table 1). This result indicates that, through adjustment of the molar ratio between TA–PEG–Gal and TA–PEG in the feed solution, the Gal density on the gold surface can be well controlled in a range of 0%–60%.

© 2013 WILEY-VCH Verlag GmbH & Co. KGaA, Weinheim

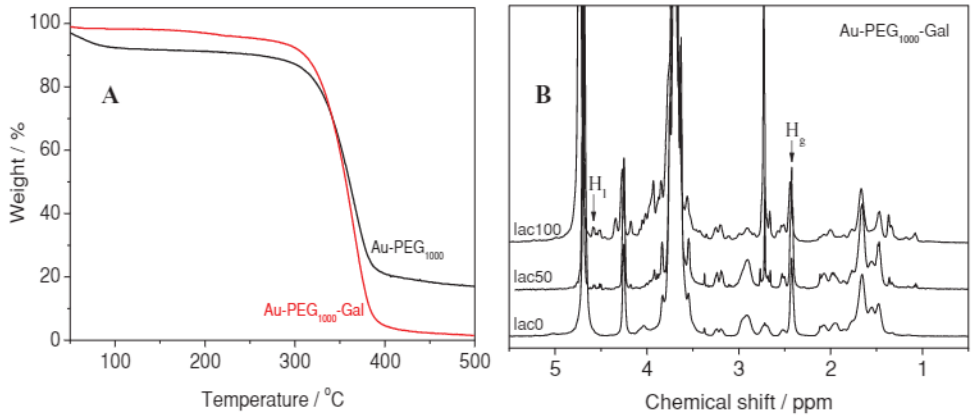

Figure 3. A) TGA curves of Au–PEG_{1000} and Au–PEG_{1000}–Gal and B) ^{1}H NMR spectra of Au–PEG_{1000}–Gal with TA–PEG_{1000}–Gal molar percentage of 100%, 50%, and 0%.

The optical properties of the as-prepared gold nanoparticles were characterized using UV–vis spectroscopy (**Figure 4**A). The citrate-stabilized gold nanoparticles display a characteristic UV–vis absorption spectrum with a surface-localized plasmon resonance band at 510 nm (Figure 4A, dotted curve), which reflects the existence of gold nanoparticles with diameters of approximately 5–6 nm. The UV–vis spectra of the PEG-derivatized gold nanoparticles exhibit an absorption band at approximately 518 nm (Figure 4A, dashed curve). This red-shift absorption band implies the formation of Au–S bonds on the surface of the gold nanoparticles. When the Gal moiety is modified on the outer shell of the gold conjugates, the absorption band is further red-shifted to ca. 527 nm, and this shift may be due to the formation of intermolecular hydrogen bonds between the carbohydrate molecules. This phenomenon can be explained by transmission electron microscopy (TEM) images of the citrate-protected gold nanoparticles, Au–PEG_{400}, and Au–PEG_{400}–Gal, which are shown in Figure 4B–D (TEM results of the same samples whose UV–vis spectra are shown in Figure 4A, a–c). The gold nanoparticles are spherical with a uniform diameter of approximately 5 nm (Figure 4B). After PEGylation, the size and shape of the Au–PEG conjugates do not significantly change. The increased interparticle distance of the PEG-modified gold particles may be due to the presence of polymer chains of PEG (Figure 4C). In contrast, the distance between the Gal-terminated gold conjugates is shorter than that of the PEGylated gold nanoparticles (Figure 4D), which indicates that a hydrogen-bonding effect may exist between the Gal moieties on the surface of Au–PEG–Gal. The result is consistent with the shift of the surface plasmon resonance absorption of the galactose–PEGylated gold nanoparticles.

2.2. Stability Assay

To evaluate the stability of the gold conjugates in different environments that immediately induced aggregation of unmodified gold particles, the UV–vis absorption intensity at 520 nm as a function of time was measured. The results are shown in **Figure 5**. The decay of the optical absorbance of the particle suspension at 520 nm is negligible for the Au–PEG–Gal conjugate (a) in 0.03 M PBS at a pH of 7.4. The relative absorbance of each group at 12 h is no less than 75% of those of the gold conjugates at 0 h, which indicates that the conjugates are stable in buffers with lower pH values (pH 5.5, b), elevated salt concentrations (0.2 M PBS, pH 7.4, c), and even in the presence of serum (d).

2.3. Biocompatibility Assay

The biocompatibility of conjugates was tested using the classic 3-(4,5)-dimethylthiahiazo(-z-y1)-3,5-di-phenytetrazoliumromide (MTT) method. The percentage of cell viability as a function of different gold concentrations is shown in **Figure 6**. In the case of HeLa cells, the viability of the cells is high and no significant

Table 1. Gal molar percentage on the gold nanoparticle surface.

Sample	Molar percentage of TA–PEG–Gal:TA–PEG in conjugate preparation	PEG–Gal ligand molar percentage on the gold surface by ^{1}H NMR [%]		
		Au–PEG_{400}–Gal	Au–PEG_{600}–Gal	Au–PEG_{1000}–Gal
Lac100	100:0	59.70	60.42	63.09
Lac75	75:25	23.45	21.14	24.27
Lac50	50:50	10.20	7.25	6.71
Lac25	25:75	5.35	4.76	3.23
Lac0	0:100	0	0	0

© 2013 WILEY-VCH Verlag GmbH & Co. KGaA, Weinheim

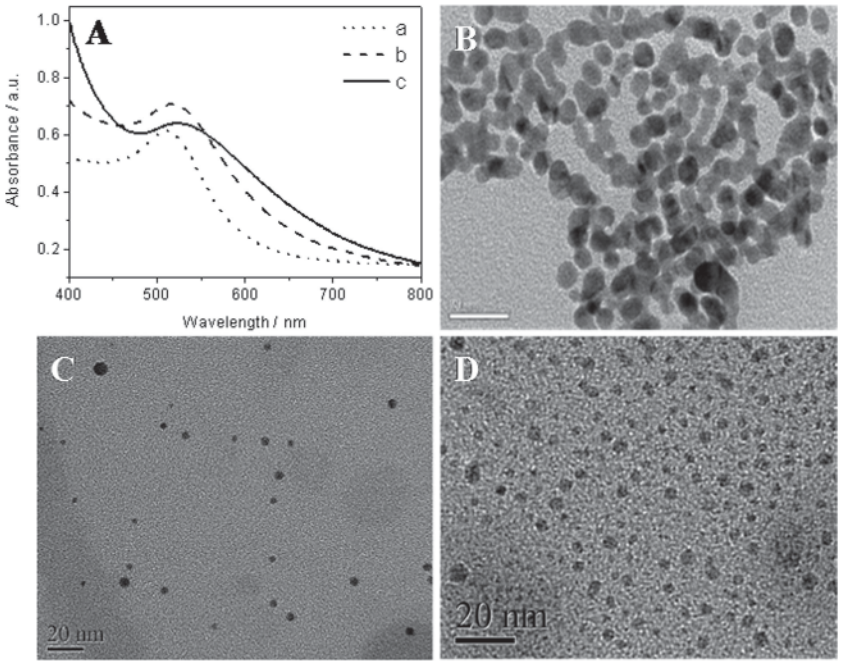

Figure 4. A) UV–vis spectra and TEM images of B) citrate-protected gold nanoparticles, C)Au–PEG_{400}, and D)Au–PEG_{400}–Gal (Lac50).

differences are observed between the surface modification and the concentration of gold conjugates, which means that HeLa cells are sensitive neither to the amount of gold conjugates nor to the modification of the galactose moiety (Figure 6A). On the contrary, when the concentration of gold is increased from 0.84 to 107.10 μg mL^{-1}, the percentage viability of the HepG2 cells decreases by 70% (from ca. 90% to 20%). These phenomena indicate that the HepG2 cells are more sensitive to the existence of gold conjugates than the HeLa cells, and that the enhancement of gold concentration and the presence of the Gal moiety would lead to high cytotoxicity in HepG2 cell lines. The

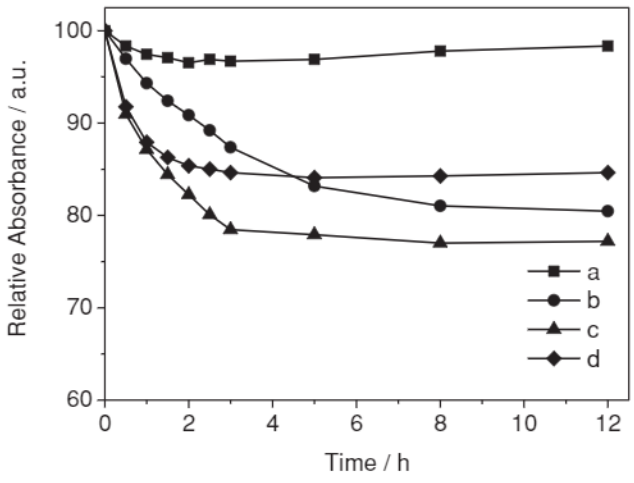

Figure 5. Dispersion stability of Au–PEG_{1000}–Gal as a function of time in various environments: in 0.03 M PBS at pH 7.4 (a), in 0.03 M PBS at pH 5.5 (b), in 0.2 M PBS at pH 7.4 (c), and in 0.03 M PBS with 2% serum (d).

IC_{50} values for the Au–PEG_{400}, Au–PEG_{400}–Gal (Lac50), and Au–PEG_{1000}–Gal (Lac50) are determined to be 17.4 ± 1.5, 11.3 ± 1.1, and 5.3 ± 0.9 μg mL^{-1}, respectively. The low cytotoxicity of Au–PEG_{400} sample can be due to the low cellular uptake and subsequent less accumulation of gold nanoparticles in HepG2 cells, which could be attributed to the lack of liver-targeting moiety on the gold surface. The galactose-modified gold conjugates with the same MW of 400 Da showed better biocompatibility than that of conjugates with PEG chain of 1000 Da, even when they have similar Gal densities. It could be due to the toxicity from either the long chain of PEG molecules or the relative large size of gold conjugates, which is not clear yet.

2.4. Cellular Uptake and Light-Scattering Imaging

Gold particle suspensions are known to scatter colored light when illuminated with a beam of white light.[28] To evaluate the influence of PEG MW, Gal density, gold concentration, and the presence of lactose on the cellular uptake efficiency in HepG2 cells, dark-field images of cells are taken using a simple optical microscope with an Olympus film camera. As shown in **Figure 7**A-1–C-1,D-1–F-1, the dark-field images for the HepG2 cells incubated with Au–PEG_{400}–Gal and Au–PEG_{1000}–Gal with different Gal densities show different light-reflectance intensities. The results provide several clues with respect to the cellular uptake properties of the Au conjugates. First, when the PEG MW is unchanged, the light reflectance of gold conjugates shows dependence of the Gal density, and the highest Gal density gives the strongest light reflectance (Figure 7A-1,D-1). In addition, the light-reflectance images for the groups incubated with gold conjugates without the Gal moiety [Au–PEG_{400} (Lac0) and Au–PEG_{1000} (Lac0) in Table 1] are shown in Figure 7C-1,F-1, showing weak light reflection. This result indicates that the existence of the Gal group on the surface of the gold nanoparticles increases their cellular uptake, which is possibly due to the ASGPR-mediated endocytosis mechanism. Moreover, for gold conjugates with a similar Gal density level but with a different PEG MW, the one with a shorter PEG chain (such as Au–PEG_{400}–Gal) shows a higher cellular uptake efficiency than the Au–PEG_{1000}–Gal. For example, the image for Au–PEG_{400}–Gal (Lac100) with a Gal modification of approximately 56.18% (Figure 7A-1) shows a light-scattering intensity stronger than that of Au–PEG_{1000}–Gal (Lac100) with a Gal density of 62.04% (Figure 7D-1). In addition, the Au–PEG_{400}–Gal (Lac100) group shows the strongest light reflectance of gold scattering in HepG2 cells, which may be due to the high surface substitution of the galactose group and the hydrophobic interaction with the cell membrane induced by the short polyethylene glycol chain.

To confirm the ASGPR-mediated cellular uptake mechanism for the Gal-bearing gold nanoparticles, the control groups

© 2013 WILEY-VCH Verlag GmbH & Co. KGaA, Weinheim

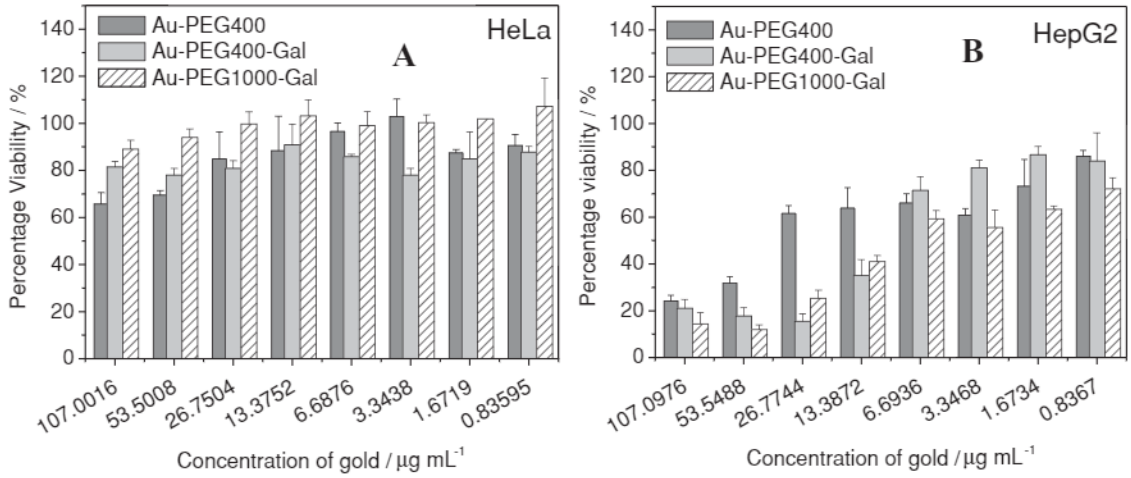

Figure 6. In vitro cytotoxicity of Au–PEG_{400}, Au–PEG_{400}–Gal (Lac50), and Au–PEG_{1000}–Gal (Lac50) on A) HeLa and B) HepG2 cell lines as determined by MTT assay. The percentage of the viability of cells was expressed relative to control cells ($n = 5$). The results are represented as the mean ± standard deviation.

for the cellular uptake of gold conjugates in HepG2 cells in the presence of free lactose (75×10^{-3} M) were determined (Figure 7A-2–C-2 for Au–PEG_{400}–Gal samples and D-2–F-2 for Au–PEG_{1000}–Gal samples). A comparison of these results with those for the test groups without the addition of free lactose, the scattering light intensity of gold for each control group decreases significantly, and, in some groups, the light is difficult to observe. This phenomenon indicates that the ASGPR-induced cellular uptake process of the gold conjugates is inhibited in HepG2 cells, and it can also explain the Gal-density-dependent uptake efficiency of gold conjugates through the ASGPR-mediated endocytosis mechanism.

To demonstrate that the hydrophobic interaction induced by the short PEG chain with the cell membrane can enhance the cellular uptake efficiency, HeLa cells with low expression of ASGPR were used to evaluate the cellular uptake of gold conjugates with similar Gal densities and different PEG MWs. As shown in Figure S1 (Supporting Information), HeLa cells incubated with Au–PEG_{400}–Gal (Lac100) display a brighter light-scattering signal than the gold conjugates with longer PEG chains, such as Au–PEG_{600}–Gal (Lac100) and Au–PEG_{1000}–Gal (Lac100). This result indicates short PEG chain has the ability to enhance the cellular uptake efficiency, which may be due to the hydrophobic interaction with the cell membrane.

In addition to the PEG MW and Gal density, the gold concentration in the gold conjugates applied to the HepG2 cells can also affect the cellular uptake capability of the gold conjugates. The dark-field images for the Au–PEG_{1000}–Gal (Lac0 and Lac50) and Au–PEG_{400}–Gal (Lac50) in different gold concentrations (0.4, 0.8, and 1.6 μg mL^{-1}) are shown in Figure S2 (Supporting Information). For the Au–PEG sample (Figure S2, A1–A3, Supporting Information), the light-scattering intensity does not obviously change as the gold concentration increases. This

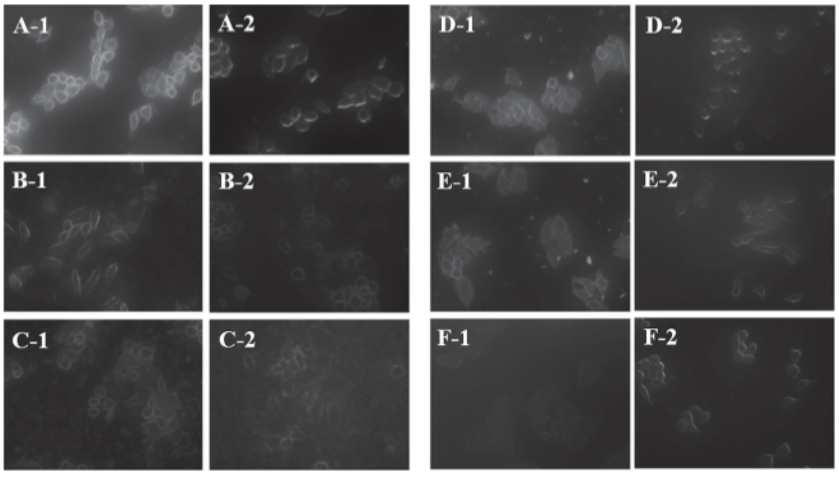

Figure 7. Dark-field microscopy images of HepG2 cells in A-1–F-1) the absence or A-2–F-2) presence of 75×10^{-3} M lactose incubated with A–C)Au–PEG_{400}–Gal and D–F)Au–PEG_{1000}–Gal with a decreased Gal density of Lac100, Lac25, and Lac0, respectively, at 37 °C for 4 h.

© 2013 WILEY-VCH Verlag GmbH & Co. KGaA, Weinheim

result implies that, without the help of specific galactose ligand recognition by the ASGPR, the cellular uptake efficiency does not increase significantly even when the gold concentration is enhanced. On the contrary, based on the light-scattering intensity in the images (Figure S2, B1–B3, C1–C3, Supporting Information), an increase in the gold concentration in gold conjugates results in brighter dark-field images for the Au–PEG–Gal samples bearing the galactose moiety. These phenomena demonstrate that, with both the PEG MW and the Gal density held constant, the cellular uptake efficiency is dependent on the gold concentration in the gold conjugates. Moreover, the Au–PEG_{400}–Gal sample with a high gold concentration of 1.6 μg mL^{-1} exhibits the strongest light-scattering intensity (Figure S2, C3, Supporting Information), which is consistent with the previously discussed results relating to the effect of short PEG chain.

2.5. Biodistribution Study

In the biodistribution study of the comprehensive consideration of the toxicity and cellular uptake capabilities, the Au–PEG_{400}–Gal (Lac50) sample was selected for an evaluation of the liver-targeting ability of the gold conjugates. The blood and tissue distribution results of gold nanoparticles and gold conjugates with and without the Gal moiety are shown in **Figure 8**. Within the study period of 48 h, as shown in Figure 8A, citrate-protected gold nanoparticles show a low gold concentration in the blood and are mainly accumulated in the liver and spleen, which could be attributed to the opsonization effect.[29] In the case of Au–PEG_{400} (Figure 8B), PEG modification obviously increases the gold content in the blood, and, at the same time, the gold content in the liver and spleen relatively decreases. These results indicate the stealth and long-circulating effects that arise from the polyethylene glycol molecules.[30] Although the gold contents in the liver and spleen for the Au–PEG_{400} group are lower than the citrated-stabilized gold nanoparticles at all the same time points, a trend is evident with respect to increasing time, and the maximum is achieved at 48 h. In addition, an almost threefold increase in the gold concentration in the kidney for the Au–PEG_{400} group is found in comparison with the concentration of citrate-protected gold nanoparticles. These phenomena imply that small nanoparticles such as Au–PEG_{400} finally accumulate in the liver and spleen and are eliminated by the kidney. Different from the results for citrate- and PEG_{400}-protected gold nanoparticles, the Au–PEG_{400}–Gal (Lac50) bearing the galactose moiety on the surface shows a higher liver intake of gold nanoparticles, which maintains a high level from 1 to 48 h (Figure 8C). This result indicates that, with its galactose-targeting function and high ASGPR affinity, Au–PEG_{400}–Gal is rapidly targeted to liver tissue and has a strong interaction with liver cells, which proves the active liver-targeting property of the Au–PEG–Gal particles. The reason for the small increase in the gold content in the lung of the Au–PEG_{400}–Gal group compared with that of the Au–PEG_{400} group is not immediately clear, which is attributed, in part, to the long circulation and small size effect of gold nanoparticles.

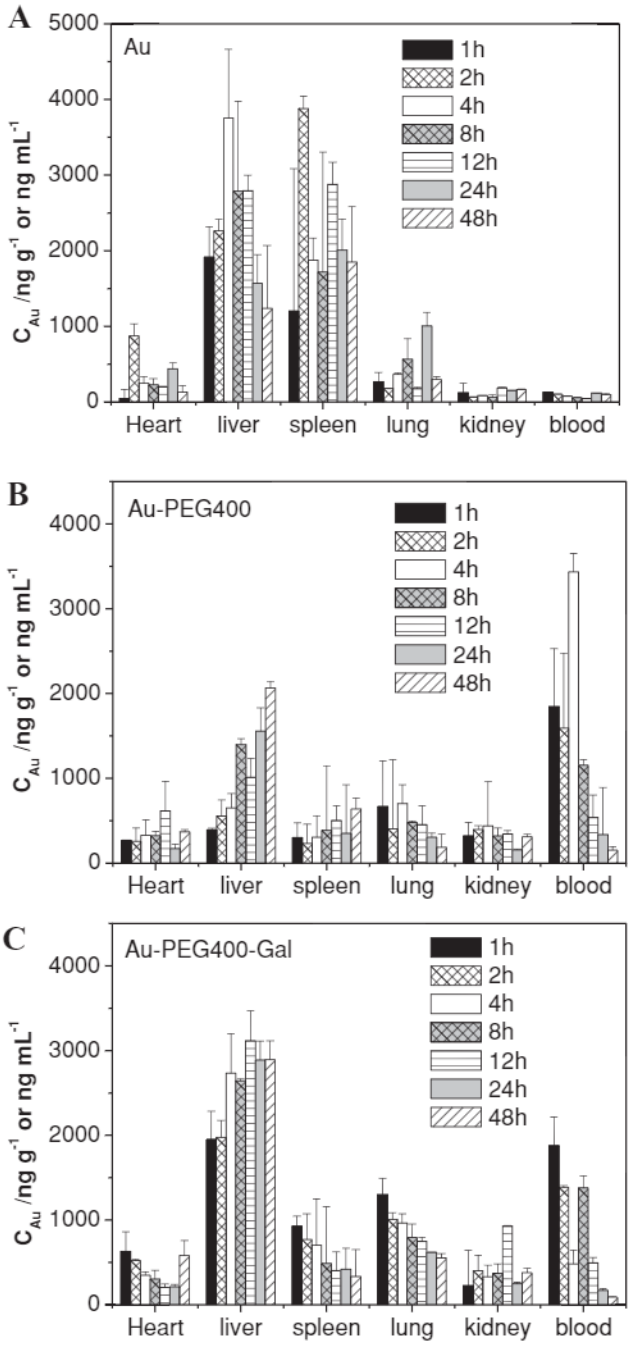

Figure 8. Biodistribution of gold in mice treated with A) citrate-protected gold nanoparticles, B)Au–PEG_{400} (Lac0), and C)Au–PEG_{400}–Gal (Lac50) in different organs of mice at various time points after intravenous injection. The values were acquired as the percentage of ID per gram of collected organs and were based on three mice per group.

3. Conclusion

In this work, a gold nanoparticle probe for liver targeting and reflectance imaging has been fabricated on the basis of a simple method. For the construction of gold conjugates, the MW of PEG molecules employed for the synthesis of functional ligands has been restricted no more than 1000 Da (in this case 400, 600,

© 2013 WILEY-VCH Verlag GmbH & Co. KGaA, Weinheim

and 1000 Da), and the density of target moiety (galactose in this work) on the gold surface can be well controlled in the range of 0%–60%. The prepared gold conjugates show high stability and maintain the optical properties of gold nanoparticles. The biocapability results showed that HepG2 cells are more sensitive than HeLa cells to the gold conjugates possibly due to the special recognition between the ASGPR in the cell membrane of HepG2 cells and the galactose-modified gold nanoparticles. The cellular uptake studies showed that a low PEG MW, a high Gal density, or a high gold concentration increased the cellular uptake efficiency of these gold conjugates in HepG2 cells when the other two parameters were unchanged. The biodistribution study results determined by ICP-MS method showed that the prepared gold conjugates with relatively short PEG chains and a relatively high Gal density showed obvious accumulation in the liver in comparison with gold nanoparticles protected by either citrate or PEG_{400}. In addition, although the short chain of PEG molecules (MW = 400) has been employed, the gold conjugates showed long circulation times compared with citrated-protected gold nanoparticles during 48 h in vivo. These results reveal the importance of parameter modulation in the design and control of nanoprobes such as sugar-functionalized gold nanoparticles, and the prepared gold conjugates with short PEG chains and a high Gal density are a potential vector for active-targeting therapy, especially liver cancer treatment.

4. Experimental Section

Materials and Instruments: Hydrogen tetrachloroaurate hydrate ($HAuCl_4{\cdot}3H_2O$) was obtained from Shanghai Chemical Regent Company (China). Polyethylene glycol (with a MW of 400, 600, or 1000 Da), DCC, and DMAP were obtained from Sigma Ltd. (USA). TA (99%) was purchased from Nanjing Zelang Pharmaceutical Technology, and Sinopharm Chemical Reagent (China). Unless otherwise stated, all starting materials were obtained from commercial suppliers and were used without further purification. Solvents were dried using standard procedures. All aqueous solutions were prepared using deionized water (>18 MΩ; Purelab Classic Corp., USA).

All gold conjugates were measured with a JEM-200CX TEM and a Tecnai F30 instrument (Philips-FEI, The Netherlands) operated at an accelerating voltage of 200 kV. UV–vis spectra were recorded on a UV-2401 PC UV/vis spectrophotometer (Shimadzu, USA). The chemical structures of intermediates and compounds in KBr discs were determined using a Tensor-27 FT-IR spectrometer (Bruker, USA) equipped with a liquid-nitrogen-cooled mercury cadmium telluride (MCT) detector. ^1H and ^{13}C NMR spectra of all organic intermediates and final products were recorded on a Bruker AVANCE AV-500 spectrometer. TGA was conducted on a thermogravimetric analyzer (TG 209 F1, Netzsch, Germany). The light-reflectance images were recorded using an inverted Olympus IX71 microscope for the cellular uptake observations.

Preparation of Citrate-Protected Gold Nanoparticles: Citrate-protected gold nanoparticles were synthesized in a single-phase system[24,25] of filtered sub-boiling water through a microporous membrane with an aperture of 0.22 µm. All glassware were cleaned in a bath of freshly prepared aqua regia and then rinsed thoroughly with deionized water prior to use. Hydrogen tetrachloroaurate(III) trihydrate (0.3 mL, 49.0×10^{-3} M) and solid sodium citrate (50 mg, 1.3 mmol) were dissolved in 25 mL of triply distilled H_2O. A freshly prepared and cooled aqueous solution of sodium borohydride (1.2 mL, 0.1 M) was added to the reaction solution, resulting in immediate color change to pink. After vigorous stirring for 30 min, the resulting solution was obtained as a burgundy-red colloidal dispersion of gold.

Synthesis of Functional Polyethylene Glycol Ligands (TA–PEG and TA–PEG–Gal): A general synthesis method was used to obtain all intermediates and final products with PEG MWs of 400, 600, and 1000 (shown in Figure 1). The synthesis procedure for the TA–PEG_{400}–Gal ligand is described as an example.

TA–PEG_{400}: PEG_{400} (12 g, 30 mmol), TA (1.23 g, 6 mmol), and DMAP (0.30 g, 2.4 mmol) were dissolved in 25 mL of dichloromethane (DCM). The reaction mixture was protected by N_2 and cooled to 0 °C in an ice bath. A solution of DCC (2.47 g, 12 mmol) in 25 mL of DCM was added slowly. After stirred for 1 h at 0 °C, the reaction mixture was stirred at room temperature for 24 h. The reaction solution was filtered, and the organic layer was concentrated. The resulting viscous solution was mixed with saturated sodium carbonate (Na_2CO_3) solution followed by extraction with ethyl acetate until TA–PEG_{400} was completely extracted from the aqueous layer. The organic extract was dried over sodium sulfate (Na_2SO_4), filtered, and evaporated to give a yellow oil. This crude product was further purified by column chromatography (CH_2Cl_2:MeOH = 40:1) and evaporated to give 2.0 g (56.8%) as a yellow oil. ^1H NMR (500 MHz, $CDCl_3$): δ 1.48 (m, 2H), 1.69 (m, 4H), 1.92 (m, 1H), 2.38 (m, 2H), 2.41 (s, broad, OH), 2.45 (m, 1H), 3.15 (m, 2H), 3.62–3.75 (m, 36H, broad), 4.25 (m, 2H). ^{13}C NMR (500 MHz, $CDCl_3$): δ 24.50, 28.60, 33.83, 34.48, 38.37, 40.10, 56.12, 61.59, 63.35, 69.05, 70.20, 70.45, 72.51, 173.31.

TA–PEG_{600}: ^1H NMR (500 MHz, $CDCl_3$): δ 1.48 (m, 2H), 1.69 (m, 4H), 1.92 (m, 1H), 2.35 (t, 2H), 2.47 (m, 1H), 3.13 (m, 2H), 3.60–3.73 (m, 55H), 4.23 (m, 2H). ^{13}C NMR (500 MHz, $CDCl_3$): δ 24.40, 28.47, 33.72, 34.36, 38.26, 39.99, 53.31, 56.10, 61.46, 63.23, 68.94, 70.13, 70.36, 72.36, 173.15.

TA–PEG_{1000}: ^1H NMR (500 MHz, $CDCl_3$): δ 1.46 (m, 2H), 1.66 (m, 4H), 1.92 (m, 1H), 2.35 (m, 2H), 2.37 (m, 1H), 2.46 (m, 1H), 3.18 (m, 2H), 3.54–3.73 (m, 90H), 4.24 (m, 2H). ^{13}C NMR (500 MHz, $CDCl_3$): δ 24.46, 28.54, 33.78, 34.43, 38.32, 40.05, 56.16, 61.52, 63.30, 69.01, 70.15, 70.41, 72.48, 173.25.

Glycine was protected by Boc group using a classical method reported previously to yield of the product (84.7%) as a white powder.[31]^1H NMR (500 MHz, $CDCl_3$): δ 1.44 (s, 9H), 3.91 (d, 2H), 5.19 and 6.65 (s, 1H, broad), 11.07 (s, 1H, broad). ^{13}C NMR (500 MHz, $CDCl_3$): δ 28.25, 42.21, 80.42, 156.03, 174.65.

TA–PEG_{400}–Gly–Boc: TA–PEG_{400} (588 mg, 1.0 mmol), Boc–Gly (210 mg, 1.2 mmol), DCC (312 mg, 1.5 mmol), and DMAP (16 mg, 0.13 mmol) were dissolved in DCM (15 mL). After stirred at room temperature for 24 h, the reaction solution was filtered, and the organic layer was concentrated. The resulting viscous solution was mixed with saturated Na_2CO_3 solution and then extracted with ethyl acetate until TA–PEG_{400}–Gly–Boc was completely extracted from the aqueous layer. The organic extract was dried over Na_2SO_4, filtered, and evaporated to yield a yellow oil. The crude product was further purified by column chromatography (CH_2Cl_2:MeOH = 30:1) and evaporated to give 0.60 g (80.1%) as a yellow oil. ^1H NMR (500 MHz, $CDCl_3$): δ 1.45 (m, 9H), 1.50 (m, 2H), 1.68 (m, 4H), 1.85 (m, 1H), 2.35 (t, 2H), 2.49 (m, 1H), 3.18 (m, 2H), 3.58 (m, 1H), 3.60–3.80 (m, 34H), 3.93 (s, 2H, broad), 4.22 (t, 2H), 4.30 (t, 2H), 5.13 (s, 1H, broad). ^{13}C NMR (500 MHz, $CDCl_3$): δ 24.41, 28.14, 28.49, 33.73, 34.38, 38.27, 40.00, 42.22, 56.13, 63.25, 64.10, 68.96, 70.37, 70.42, 79.62, 155.55, 170.17, 173.17.

TA–PEG_{600}–Gly–Boc: ^1H NMR (500 MHz, $CDCl_3$): δ 1.45 (m, 9H), 1.50 (m, 2H), 1.72 (m, 4H), 1.92 (m, 1H), 2.35 (t, 2H), 2.49 (m, 1H), 3.18 (m, 2H), 3.58 (m, 1H), 3.60–3.80 (m, 40H), 3.93 (s, 2H, broad), 4.22 (t, 2H), 4.30 (t, 2H), 5.30 (s, 1H, broad). ^{13}C NMR (500 MHz, $CDCl_3$): δ 24.48, 28.20, 28.56, 33.80, 34.45, 38.34, 40.07, 42.29, 56.18, 63.32, 64.18, 68.77, 69.03, 70.44, 70.49, 79.73, 155.61, 170.25, 173.25.

TA–PEG_{1000}–Gly–Boc: ^1H NMR (500 MHz, $CDCl_3$): δ 1.45 (m, 9H), 1.50 (m, 2H), 1.65 (m, 4H), 1.88 (m, 1H), 2.20–2.31 (d, 2H, broad), 2.31 (m, 2H), 2.47 (m, 1H), 3.13 (m, 2H), 3.45–3.80 (m, 83H), 3.90 (s, 2H), 4.21 (t, 2H), 4.28 (t, 2H), 5.13 (s, 1H, broad). ^{13}C NMR (500 MHz, $CDCl_3$): δ 24.51, 28.23, 28.59, 33.83, 34.48, 38.36, 40.10, 42.32, 56.21, 63.35, 64.20, 68.79, 69.06, 70.47, 79.77, 155.64, 170.28, 173.29.

The deprotection of Boc group on TA–PEG–Gly–Boc used trifluoroacetic acid (TFA)[31] according to the previous report and yielded

© 2013 WILEY-VCH Verlag GmbH & Co. KGaA, Weinheim

1.24 g (79.6%) of the product as a yellow oil. ^{1}H NMR (500 MHz, $CDCl_3$): δ 1.48 (m, 2H), 1.64 (m, 4H), 2.01 (m, 1H), 2.78 (t, 1H), 3.13 (m, 2H), 3.61–3.71 (m, 28H), 4.22 (t, 2H), 4.28 (t, 2H). ^{13}C NMR (500 MHz, $CDCl_3$): δ 24.47, 24.62, 25.56, 26.55, 28.56, 29.53, 30.70, 31.60, 33.80, 34.44, 38.33, 40.07, 42.26, 56.18, 61.41, 63.31, 69.01, 70.03, 70.37, 72.48, 173.30.

TA–PEG$_{600}$–Gly: ^{1}H NMR (500 MHz, $CDCl_3$): δ 1.48 (m, 2H), 1.72 (m, 4H), 1.89 (m, 1H), 2.35 (t, 2H), 2.45 (m, 1H), 3.18 (m, 1H), 3.55–4.00 (m, 49H), 4.22 (t, 2H), 4.28 (t, 2H). ^{13}C NMR (500 MHz, $CDCl_3$): δ 24.50, 24.85, 28.58, 29.55, 30.93, 33.82, 34.47, 38.35, 40.09, 43.66, 53.34, 56.21, 61.53, 63.34, 63.86, 68.90, 69.05, 70.18, 70.45, 72.44, 173.28.

TA–PEG$_{1000}$–Gly: ^{1}H NMR (500 MHz, $CDCl_3$): δ 1.45 (m, 2H), 1.72 (m, 4H), 1.80–1.95 (m, 1H), 2.35 (t, 2H), 2.45 (m, 1H), 2.78 (s, 3H), 3.18 (m, 1H), 3.46 (m, 1H), 3.55–4.00 (m, 67H), 4.22 (t, 2H), 4.28 (t, 2H). ^{13}C NMR (500 MHz, $CDCl_3$): δ 24.53, 24.63, 24.87, 25.57, 28.61, 29.58, 33.85, 34.50, 38.38, 40.12, 43.59, 53.35, 56.23, 61.57, 63.37, 63.92, 69.08, 70.21, 70.48, 72.46, 173.30.

TA–PEG$_{400}$–Gal: TA–PEG$_{400}$–Gly (75 mg, 0.12 mmol) and LA (72 mg, 0.20 mmol) were dissolved in dimethyl sulfoxide (DMSO; 8 mL) and stirred for 2 h. *N*-hydroxysulfosuccinimide sodium salt (NHS; 96 mg, 0.83 mmol) and 1-ethyl-3-(3-dimethylaminopropyl)carbodiimide hydrochloride (EDC·HCl; 173 mg, 0.90 mmol) were added, and the mixture was stirred for 3 d. The as-prepared solution was used for the surface conjugation of gold nanoparticles without any purification. TA–PEG$_{600}$–Gal and TA–PEG$_{1000}$–Gal were synthesized according to the previously described method for the synthesis of TA–PEG$_{400}$–Gal.

Au–PEG–Gal Conjugate Synthesis and Stability Analysis: The dithiolane group in TA–PEG ligands with and without the Gal moiety was conjugated to gold surfaces via a ring-opening reaction via the sodium borohydride ($NaBH_4$) reduction method.[26] To a 2-mL methanol solution of ligands (0.12 mmol), in which the PEG molar weights of derivatives were 400, 600, and 1000 Da and the molar ratio of TA–PEG/TA–PEG–Gal was set to be in the range of 0%–100% (shown in Figure 1), 1.5 equiv. of $NaBH_4$ (6.8 mg, 0.18 mmol) in 1 mL of ice water was added. The solution was stirred for 1 h at 4 °C and acidified to pH 6 with 1 mol L^{-1} HCl. The linkage of S–Au bond was performed by the addition of citrate-stabilized gold nanoparticles into the reaction solution at gold/ligand molar ratio of 1:1000. The resultant liquid was dialyzed in regularly refreshed deionized water for 24 h (molar weight cutoff, MWCO = 3500) and lyophilized to give light-red powder or viscous substance of gold conjugates (denoted as Au–PEG and Au–PEG–Gal, respectively) according to the PEG MW. The products readily dissolved in water and in phosphate-buffered solutions (PBSs).

For stability analysis, gold conjugates were incubated at 37 °C under the following conditions: the as-prepared pH (0.03 M PBS at pH 7.4); the pH lowered to 5.5 by the addition of concentrated HCl; the higher ionic strength of 0.2 M PBS at pH 7.4; and in the presence of plasma (at pH 7.4 in 0.03 M PBS solution with 2% plasma). Absorbance of the conjugates at a wavelength of 520 nm was monitored at designed time points.

Cell Culture, Light-Scattering Labeling, and Microscopy: HepG2 (human hepatoblastoma) and HeLa (human cervical cancer) cells were originally obtained from the Chinese Academy of Sciences (Shanghai, China). The cells were cultured in Dulbecco's modified Eagle's medium (DMEM), and incubated at 37 °C under a humidified 5% CO_2 atmosphere. The cells were split to approximately 80% confluency in a 96-well culture plate the day preceding the assay. The cells were incubated for 4 h with Au–PEG and Au–PEG–Gal samples at a final gold concentration of 9 μg mL^{-1}. After the incubation process, the cells were washed three times with 1 mL of cold PBS, and the cellular uptake and reflectance imaging of the gold conjugates were analyzed using dark-field microscopy with a narrow beam of white light at 100× magnification.

Biocompatibility Assay: HepG2 and HeLa cells (5×10^4 cells) were cultivated in a 96-well plate at 37 °C under a 5% CO_2 atmosphere. After 24 h, the medium was replaced with fresh medium that contained the Au–PEG and Au–PEG–Gal conjugates in various concentrations. After cultivation again for 24 h, 10 μL of MTT dye solution (5 mg mL^{-1} in PBS) was added to each well. After 4 h of incubation at 37 °C and under a 5% CO_2 atmosphere, the medium was removed, the cells were washed with PBS, and formazan crystals were dissolved in 100 μL of DMSO. The absorbance of each well was read on a microplate reader (Thermo Multiskan Mk3, Thermo Fisher Scientific, USA) at 570 nm. The spectrophotometer was calibrated to zero absorbance using culture medium without cells. The relative cell viability (%) relative to control wells that contained cell culture medium without gold conjugates was calculated according to the equation $[A]_{test}/[A]_{control} \times 100$.

Biodistribution Study: Institute for Cancer Research (ICR) male mice (body weight of 25–30 g) used in this study were purchased from Zhejiang Experimental Animal Center (China) and were housed in stainless steel cages in a ventilated animal room. Room temperature was maintained at 20 ± 2 °C, relative humidity was maintained at 60 ± 10%, and a 12-h light/dark cycle was used. Distilled water and sterilized food for mice were available ad libitum. The mice were acclimated to this environment for 5 d prior to dosing. All animal procedures were performed in compliance with the regulations and guidelines of the National Ethics Committee on Animal Welfare of China.

On the day of experiments, mice were grouped into separate cages (n = 3). Mice were anesthetized with light ether. Citrate-protected gold nanoparticles, Au–PEG$_{400}$ (Lac0), and Au–PEG$_{400}$–Gal (Lac50) were injected intravenously at a dose of 1.93 mg of gold kg^{-1}. The volume of injection was adjusted to 3 mL per 100 g of mice weight. The injections were well tolerated, and no adverse effects were observed during the 48 h observation period. At the time points of 1, 2, 4, 8, 12, 24, and 48 h postadministration, the mice were anesthetized with light ether. Blood was collected through the retro orbital plexus region in a heparinized glass tube. The mice were subsequently sacrificed by cervical dislocation, and tissues, including the heart, liver, spleen, lung, and kidney, were collected. The tissues were briefly washed with normal saline and dried with blotting paper. The isolated tissues were weighed accurately and were stored at –20 °C. The tissue powder was obtained using the freeze-drying method. Blood was stored in a refrigerator at 4–6 °C until being assayed.

All tissue powders were separately nitrified in 2 mL of aqua regia in screwcap glass bottles (15 mL). The residual aqua regia was evaporated by heating at 100 °C in an oil bath for 6 h. The residue was then redissolved in 1% diluted HNO_3 and hydrogen peroxide, and the resultant samples were analyzed via ICP-MS.

Supporting Information

Supporting Information is available from the Wiley Online Library or from the author.

Acknowledgements

This work was financially supported by grants from the National 973 Basic Research Program (2012CB933800), the Natural Science Foundation of China (30900337), the Program for New Century Excellent Talents in University (NCET-10–0816), the Doctoral Fund of Ministry of Education of China (20090096120001), the China Postdoctoral Science Foundation (2008440155, 201003566), the Fundamental Research Funds for the Central Universities (JKQ2009026, JKP2011008), the Qing Lan Project, and the Open Project Program of State Key Laboratory of Natural Medicines, China Pharmaceutical University (SKLNMKF201307).

Received: March 7, 2013
Revised: May 30, 2013
Published online: September 12, 2013

[1] M. C. Daniel, D. Astruc, *Chem. Rev.* **2004**, *104*, 293.
[2] C. S. Thaxton, D. G. Georganopoulou, C. A. Mirkin, *Clin. Chim. Acta* **2006**, *363*, 120.
[3] C. M. Cobley, J. Chen, E. C. Cho, L. V. Wang, Y. Xia, *Chem. Soc. Rev.* **2011**, *40*, 44.

© 2013 WILEY-VCH Verlag GmbH & Co. KGaA, Weinheim

[4] J. Fuente, S. Penadés, *Biochim. Biophys. Acta* **2006**, *1760*, 636.
[5] J. M. Bergen, H. A. Recum, T. T. Goodman, A. P. Massey, S. H. Pun, *Macromol. Biosci.* **2006**, *6*, 506.
[6] M. Mammen, S. K. Choi, G. M. Whitesides, *Angew. Chem Int. Ed.* **1998**, *37*, 2754.
[7] A. Housni, H. Cai, S. Liu, S. H. Pun, R. Narain, *Langmuir* **2007**, *23*, 5056.
[8] Z. Deng, S. Li, X. Jiang, R. Narain, *Macromolecules* **2009**, *42*, 6393.
[9] J. M. Fuente, A. G. Barrientos, T. C. Rojas, J. Rojo, J. Caña-da, A. Fernández, S. Penadés, *Angew. Chem.* **2001**, *113*, 2317.
[10] Á. G. Barrientos, J. M. Fuente, T. C. Rojas, A. Fernández, S. Penadés, *Chem. Eur. J.* **2003**, *9*, 1909.
[11] J. M. Fuente, P. Eaton, A. G. Barrientos, M. Menéndez, S. Penadés, *J. Am. Chem. Soc.* **2005**, *127*, 6192.
[12] L. Dong, S. Gao, H. Diao, J. Chen, J. Zhang, *J. Biomed. Mater. Res.* **2008**, *84A*, 777.
[13] W. H. De Jong, W. I. Hagens, P. Krystek, M. C. Burger, A. J. A. M. Sips, R. E. Geertsm, *Biomaterials* **2008**, *29*, 1912.
[14] H. Otsuka, Y. Nagasaki, K. Kataoka, *Adv. Drug Delivery Rev.* **2003**, *55*, 403.
[15] Y. Akiyama, T. Mori, Y. Katayama, T. Niidome, *J. Controlled Release* **2009**, *139*, 81.
[16] T. Betancourt, J. D. Byrne, N. Sunaryo, S. W. Crowder, M. Kadapakkam, S. Patel, S. Casciato, L. Brannon-Peppas, *J. Biomed. Mater. Res.* **2009**, *91A*, 263.
[17] R. Gref, J. Rodrigues, P. Couvreur, *Macromolecules* **2002**, *35*, 9861.
[18] J. Lipka, M. Semmler-Behnke, R. A. Sperling, A. Wenk, S. Takenaka, C. Schleh, T. Kissel, W. J. Parak, W. G. Kreyling, *Biomaterials* **2010**, *31*, 6574.
[19] E. Wagner, *Adv. Drug Delivery Rev.* **1999**, *38*, 279.
[20] P. H. Weigel, J. H. Yik, *Biochim. Biophys. Acta* **2002**, *1572*, 341.
[21] R. J. Stockert, *Physiol. Rev.* **1995**, *75*, 591.
[22] M. Hashida, M. Nishikawa, F. Yamashita, Y. Takakura, *Adv. Drug Delivery Rev.* **2001**, *52*, 187.
[23] Y. Yang, Y. T. Zhao, T. T. Yan, M. Yu, Y. L. Sha, Z. H. Zhao, Z. J. Li, *Tetrahedron Lett.* **2010**, *51*, 4182.
[24] Y. Ding, X.-H. Xia, H.-S. Zhai, *Chem. Eur. J.* **2007**, *13*, 4197.
[25] Y. Ding, G. Gu, X.-H. Xia, Q. Huo, *J. Mater. Chem.* **2009**, *19*, 795.
[26] K. Susumu, H. T. Uyeda, I. L. Medintz, T. Pons, J. B. Delehanty, H. Mattoussi, *J. Am. Chem. Soc.* **2007**, *129*, 13987.
[27] Y. Ding, P. Zhang, X.-Y. Tang, C. Zhang, S. Ding, H. Ye, Q.-L. Ding, W.-B. Shen, Q.-N. Ping, *Polymer* **2012**, *53*, 1694.
[28] H. C. Van De Hulst, *Light Scattering by Small Particles*, Dover, New York **1981**.
[29] J. Hostetter, R. Kagan, E. Steadham, *Clin. Diagn. Lab. Immunol.* **2005**, *12*, 793.
[30] J. Lipka, M. Semmler-Behnke, R. A. Sperling, A. Wenk, S. Takenaka, C. Schleh, T. Kissel, W. J. Parak, W. G. Kreyling, *Biomaterials* **2010**, *31*, 6574.
[31] D. M. Shendage, R. Fro1hlich, G. Haufe, *Org. Lett.* **2004**, *6*, 3675.

© 2013 WILEY-VCH Verlag GmbH & Co. KGaA, Weinheim